Configuration mixing in even-even $^{148-154}$Sm within the interacting boson model

Yingxin Wu [1,*] Xiaohan Qi [1] Feng Pan [1,2,†] and Jerry P. Draayer [2]
[1]*Department of Physics, Liaoning Normal University, Dalian 116029, China*
[2]*Department of Physics and Astronomy, Louisiana State University, Baton Rouge, Louisiana 70803-4001, USA*

(Received 28 December 2023; accepted 13 March 2024; published 5 April 2024)

The interacting boson model with configuration mixing due to two-particle–two-hole excitations is applied to describe even-even $^{148-154}$Sm to investigate the cross-shell excitation effects in these nuclei. It is shown from the fitting results to the experimentally known positive-parity level energies, $B(E2)$ values, and electric quadrupole moments that the IBM configuration mixing (CM) describes these nuclei better than the IBM consistent-Q formalism without the configuration mixing. Especially, the IBM-CM fitting results to the known $B(E2)$ values are significantly improved. Furthermore, it is shown from the IBM-CM fitting results that the intruder configuration turns to be always dominant in the 0_2^+, 2_2^+, and 4_2^+ states of well-deformed ^{150,152,154}Sm. Most notably, there is a clear normal-intruder configuration crossover along the yrast line of these nuclei described by the IBM-CM.

DOI: 10.1103/PhysRevC.109.044310

I. INTRODUCTION

The interacting boson model (IBM) has been used to great success in describing medium- and heavy-mass nuclei [1]. Though more than one shape of a nucleus can be identified from the minimum nuclear potential energy with different deformation parameters in the collective model [2], it is unable to characterize the associated configurations [3]. Duval and Barrett then extended the IBM for the first time to include the simplest mixing of the normal (valence shell) configuration with the intruder configuration due to two-particle–two-hole (2p-2h) excitations from the nearest lower shell, which has been proven to be very successful in describing nuclei near a proton shell closure [4,5]. Heyde and Wood *et al.* conducted detailed studies on the configuration mixing in even-even and odd-A nuclei around proton numbers $Z \approx 50$ and $Z \approx 82$ within the IBM with configuration mixing (CM) framework [6–8] and discussed the high spin states of even-even Dy nuclei with up to six-particle and six-hole excitations [9]. In addition, the matrix coherent state method was applied to the IBM-CM to describe the shape (phase) evolution and the quantum phase transition behaviors of some nuclei [10,11]. Detailed analysis was also made on the quantum phase transitions of some even-even nuclei in the IBM-CM [12,13] and some odd-A nuclei in the interacting boson-fermion model with configuration mixing [14,15], respectively. Since there are additional particle type and hole type bosons in the 2p-2h excitations, these bosons can either be treated as the same or different types in the IBM-CM calculations. In most previous studies, they were not distinguished from each other [10,16–22], while they were considered to be different in Ref. [23]. In some special cases, exact solution of the IBM-CM may exist [24–26]. In addition, the link between the IBM-CM and a self-consistent mean-field approach based on nuclear energy density functional may be adopted to analyze the shape coexistence phenomena [27]. Very recently, one-particle and one-hole (1p-1h) excitations to the upper next-nearest major shell have been included in the IBM framework that describes both the low-lying properties and the isoscalar giant monopole and quadrupole resonance phenomena of an even-even nucleus simultaneously [28]. Generally speaking, the shape (phase) coexistence phenomena and related properties of nuclei with proton or neutron number near a closed-shell or a subshell closure are well described by the IBM-CM. However, the aforementioned articles are mainly on configuration mixing phenomena of nuclei in vibrational and transitional regions. Due to the large deformation, multiparticle-multihole excitations from the nearest lower shell are also likely to occur in well-deformed nuclei [9,29], for which the IBM-CM description may be helpful to resolve the long-term debate on the nature of the low-lying states, especially that of low-lying 0^+ states in well-deformed nuclei [30,31].

In this paper, the IBM-CM with 2p-2h excitations from the nearest lower shell is applied to describe low-lying properties of ^{148,150,152,154}Sm. Positive-parity energy levels, experimentally known $B(E2)$ values, and electric quadrupole moments of ^{148,150,152,154}Sm are fitted and compared to the experimental data and the results of the consistent-Q (CQ) formalism without the configuration mixing [32].

II. THE MODEL

We employ an algebraic approach to the IBM-CM of normal and intruder configurations [4,33]. It should be noted that here we do not distinguish proton-type bosons from neutron-

*wuyingxin0875@163.com
†daipan@dlut.edu.cn

type bosons, nor do we distinguish particle-type bosons from hole-type bosons for simplicity. The IBM-CM is based on the shell model, in which the normal (valence shell) configuration and the intruder configuration with 2p-2h excitations from the nearest lower shell span the symmetric irreducible representations (irreps) $[N]$ and $[N+2]$ of the IBM U(6) group, respectively, where N is the total number of bosons when there is no 2p-2h excitation, which is counted as the number of valence particle pairs in the valence shell in this paper. The IBM-CM Hamiltonian can be written as [34]

$$\hat{H} = \hat{P}_N \hat{H}_{\rm nor} \hat{P}_N + \hat{P}_{N+2} \hat{H}_{\rm intr} \hat{P}_{N+2} + \hat{P}_{N+2} \hat{H}_{\rm mix} \hat{P}_N + \hat{P}_N \hat{H}_{\rm mix} \hat{P}_{N+2}, \quad (1)$$

where $\hat{P}_N$ or $\hat{P}_{N+2}$ is the projection operator, which projects onto the $[N]$ or $[N+2]$ subspace. According to the CQ formalism [35],

$$\hat{H}_{\rm nor} = \epsilon_s^{(N)} \hat{N} + \left(\epsilon_d^{(N)} - \epsilon_s^{(N)}\right) \hat{n}_d - \kappa^{(N)} \hat{Q}_\chi \cdot \hat{Q}_\chi, \quad (2)$$

$$\hat{H}_{\rm intr} = \epsilon_s^{(N+2)} (\hat{N}+2) + \left(\epsilon_d^{(N+2)} - \epsilon_s^{(N+2)}\right) \hat{n}_d - \kappa^{(N+2)} \hat{Q}_\chi \cdot \hat{Q}_\chi + \Delta + b \hat{L} \cdot \hat{L}, \quad (3)$$

where $\hat{n}_d = d^\dagger \cdot \tilde{d}$, with $\tilde{d}_\mu = (-)^\mu d_{-\mu}$, is the d-boson number operator; $\hat{N} = \hat{n}_s + \hat{n}_d$, in which $\hat{n}_s = s^\dagger s$ is the s-boson number operator; $\epsilon_s^{(N)}$ ($\epsilon_s^{(N+2)}$) and $\epsilon_d^{(N)}$ ($\epsilon_d^{(N+2)}$) are single-particle energies of the s and d bosons in each configuration; $\kappa^{(N)}$ ($\kappa^{(N+2)}$) is the strength of the quadrupole-quadrupole interaction; Δ is the energy needed for the 2p-2h excitation from the nearest lower shell;

$$\hat{Q}_\chi = d^\dagger s + s^\dagger \tilde{d} + \chi (d^\dagger \times \tilde{d})^{(2)} \quad (4)$$

is the quadrupole operator, in which $(d^\dagger \times \tilde{d})^{(l)}$ with the component of the l tensor omitted represents the angular momentum coupling of the d-boson creation and annihilation operators to the angular momentum l; the last $\hat{L} \cdot \hat{L}$ term in Eq. (3) is added to get a better fit to the low-lying level energies; and the configuration mixing term is taken as

$$\hat{H}_{\rm mix} = \omega_d [(d^\dagger \times d^\dagger)^{(0)} + (\tilde{d} \times \tilde{d})^{(0)}] + \omega_s (s^{\dagger 2} + s^2). \quad (5)$$

In the following, we take $\omega_s = \omega_d = \omega$ to reduce the number of free parameters. Since only excited states of the model are concerned, the parameter $\epsilon_s^{(N)}$ can be taken arbitrarily with no influence to excited states calculated with only the d- and s-boson single-particle energy gap $\epsilon_d^{(N)} - \epsilon_s^{(N)}$ being effective for the normal configuration.

The $E2$ transition operator is defined as

$$T(E2) = q_2^{(N)} \hat{P}_N \hat{Q}_\chi \hat{P}_N + q_2^{(N+2)} \hat{P}_{N+2} \hat{Q}_\chi \hat{P}_{N+2}, \quad (6)$$

which is consistent with the CQ formalism [35], where $q_2^{(N)}$ ($q_2^{(N+2)}$) is the effective charge related parameter for each configuration. In the calculation, $q_2^{(N)} = q_2^{(N+2)} = q_2$ is assumed. Accordingly, $B(E2; L_\xi \to L'_{\xi'})$ and the electric quadurpole moment $Q(L_\xi)$ are given by

$$B(E2; L_\xi \to L'_{\xi'}) = \frac{1}{2L+1} |\langle L'_{\xi'} || T(E2) || L_\xi \rangle|^2 \quad (7)$$

and

$$Q(L_\xi) = \sqrt{\tfrac{16\pi}{5}} \langle LL,\ 20 | LL \rangle \langle L_\xi || T(E2) || L_\xi \rangle / (2L+1)^{1/2}, \quad (8)$$

respectively, where L_ξ labels the ξth excited state with the angular momentum L.

In this paper, the eigenstates $|L_\xi\rangle$ of the Hamiltonian (1) are expanded in terms of the U(6) $\supset$ SU(3) $\supset$ SO(3) basis, which can be expressed as

$$|L_\xi\rangle = \sum_{(\lambda,\mu)\varsigma} C^{(\xi,N,L)}_{(\lambda,\mu),\varsigma} |[N](\lambda,\mu)\varsigma L\rangle + \sum_{(\lambda,\mu)\varsigma} C^{(\xi,N+2,L)}_{(\lambda,\mu),\varsigma} |[N+2](\lambda,\mu)\varsigma L\rangle, \quad (9)$$

where (λ,μ) is the Elliott label for an SU(3) irrep, ς is the SU(3) $\downarrow$ SO(3) branching multiplicity label, and $C^{(\xi,N,L)}_{(\lambda,\mu),\varsigma}$ and $C^{(\xi,N+2,L)}_{(\lambda,\mu),\varsigma}$ are the expansion coefficients. In the calculation, the analytical expressions of the reduced matrix elements of s- and d-boson creation and annihilation operators in the U(6) $\supset$ SU(3) $\supset$ SO(3) basis provided in Eq. [36] and the FORTRAN code for evaluating Wigner coefficients of SU(3) $\supset$ SO(3) [37,38] are used. Moreover, occupation probability of the normal configuration $P^{(\xi,L)}_{\rm nor}$ and that of the intruder configuration $P^{(\xi,L)}_{\rm intr}$ for a given eigenstate (9) are useful for our analysis, which are given by

$$P^{(\xi,L)}_{\rm nor} = \sum_{(\lambda,\mu)\varsigma} \left|C^{(\xi,N,L)}_{(\lambda,\mu),\varsigma}\right|^2, \quad (10)$$

$$P^{(\xi,L)}_{\rm intr} = 1 - P^{(\xi,L)}_{\rm nor} = \sum_{(\lambda,\mu)\varsigma} \left|C^{(\xi,N+2,L)}_{(\lambda,\mu)\varsigma}\right|^2. \quad (11)$$

III. THE MODEL FIT TO EVEN-EVEN $^{148-154}$Sm

The low-lying properties of even-even Sm isotopes have been extensively studied in the IBM without configuration mixing [32,39–41], which shows that there is the shape (phase) evolution from the spherical [U(5)] to the axially deformed [SU(3)] phase in even-even $^{146-154}$Sm. In particular, it is shown that ^{152}Sm with neutron number $N = 90$ is a typical nucleus at the critical point of the first-order U(5)-SU(3) shape (phase) transition [42,43].

In this paper, the IBM-CM Hamiltonian (1) is adopted to fit positive-parity level energies of even-even $^{148-154}$Sm, which are also fitted by the original CQ Hamiltonian without configuration mixing for comparison. In order to reduce the number of free parameters of the IBM-CM, the 2p-2h excitation energy needed in the IBM-CM Hamiltonian (1) for each nucleus is fixed by the average of the minimum 2p-2h excitation energies from below the neutron (n) and proton (p) closed shells with $\Delta = (\Delta_{n,\rm min} + \Delta_{p,\rm min})/2$ shown in Table I. For example, $\Delta_{n,\rm min} = 2\epsilon_{n,44} - 2\epsilon_{n,40}$ and $\Delta_{p,\rm min} = 2\epsilon_{p,32} - 2\epsilon_{p,24}$ for $^{148}_{62}$Sm$_{86}$, where $\epsilon_{n,k}$ ($\epsilon_{p,k}$) is the kth neutron (proton) single-particle energy produced from a Nilsson deformed shell model code, for which the deformation parameters of each nucleus are taken from Ref. [44]. Thus, there are eight adjustable parameters in the IBM-CM Hamiltonian (1), while there are only three parameters in the CQ formalism, which are determined from a best fit to the low-lying

TABLE I. The 2p-2h excitation energy $\Delta = (\Delta_{\mathrm{n,min}} + \Delta_{\mathrm{p,min}})/2$ for $^{148-154}$Sm, where $\Delta_{n,\mathrm{min}}$ and $\Delta_{p,\mathrm{min}}$ are the minimum excitation energies from below the neutron $N = 82$ and the proton $Z = 50$ closed shells, respectively, calculated from a Nilsson deformed shell model code, and the quadrupole deformation parameter ε_2 for each nucleus [44] is also provided.

	$^{148}_{62}\mathrm{Sm}_{86}$	$^{150}_{62}\mathrm{Sm}_{88}$	$^{152}_{62}\mathrm{Sm}_{90}$	$^{154}_{62}\mathrm{Sm}_{92}$
ε_2	0.16000	0.19000	0.22000	0.25000
$\Delta_{n,\mathrm{min}}$	4.71188	3.47630	2.49830	2.93460
$\Delta_{p,\mathrm{min}}$	8.49964	8.29098	7.98050	7.48210
Δ	6.60576	5.88364	5.23940	5.20835

positive-parity level energies of even-even $^{148-154}$Sm. Once the model parameters are thus fixed, as clearly shown in Eq. (6), there is only the effective charge related parameter q_2 that is adjustable in fitting to $B(E2)$ values. The fitting quality of both the IBM-CM and the CQ formalism is measured by the parameter-dependent root-mean-square deviation σ defined by

$$\sigma = \sqrt{\frac{1}{\mathcal{N} - \mathcal{N}_0} \sum_{i=1}^{\mathcal{N}} (O_{i,\mathrm{th}} - O_{i,\mathrm{exp}})^2}, \tag{12}$$

where $\mathcal{N}$ denotes the total number of data fitted, $\mathcal{N}_0$ is the number of adjustable parameters, and $O_{i,\mathrm{th}}$ and $O_{i,\mathrm{exp}}$ are the theoretical and the corresponding experimental values of a level energy or a $B(E2)$ value, respectively.

The parameters of the IBM-CM and the CQ formalism produced from a best fit for each nucleus are shown in Table II. In the IBM-CM, with the increasing of the mass number, both $\epsilon_d^N - \epsilon_s^N$ and $\epsilon_d^{N+2} - \epsilon_s^{N+2}$ decrease with the increasing of the mass number A, while the parameter χ gradually approaches $-\sqrt{7}/2$, indicating that the U(5)-SU(3) shape (phase) transition persists in the configuration mixing description. In the CQ formalism, the model parameter $\epsilon_d - \epsilon_s$ also decreases the increasing of the mass number A, while $\chi = -\sqrt{7}/2$ for $^{148-154}$Sm is preferred in the CQ formalism, consistent with the U(5)-SU(3) description for these nuclei shown in Ref. [32].

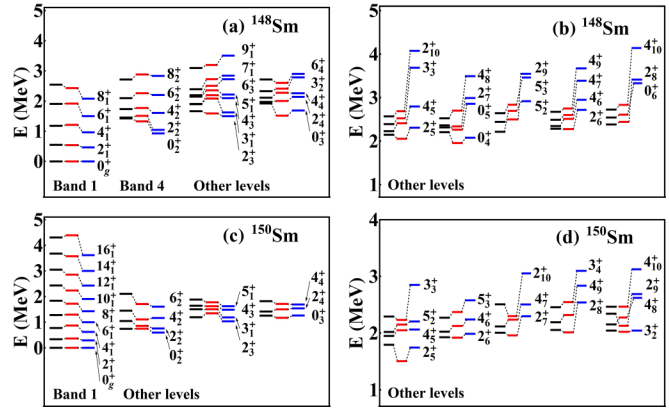

FIG. 1. Level energies (in MeV) of the experimentally identified positive-parity bands of ^{148}Sm and ^{150}Sm, where the left (black) levels are those obtained from the experiments, the middle (red) levels are those obtained from the IBM-CM, and the right (blue) levels are those obtained from the original CQ formalism.

The fitting results of both the IBM-CM and the CQ formalism to the low-lying positive-parity level energies of $^{148-154}$Sm and in comparison to the experimental results [45] are shown in Figs. 1 and 2 with the detailed data provided in Tables III–VI. For ^{148}Sm, there are 40 positive-parity levels fitted as shown in Figs. 1(a) and 1(b), among which spin and parity of the excited level at 2.441 MeV have not been determined experimentally and are assigned to be 0_6^+ in the fitting. For ^{150}Sm, there are 37 positive-parity levels fitted as shown in Figs. 1(c) and 1(d), among which spin and parity of the excited level at 2.444 MeV have not been determined experimentally and are assigned to be 5_3^+ in the fitting. For ^{152}Sm, there are 60 positive-parity levels fitted as shown in Figs. 2(a) and 2(b), among which spin and parity of the excited levels at 2.423 and 2.309 MeV have not been determined experimentally and are assigned to be 0_8^+ and 5_3^+, respectively,

TABLE II. The model parameters determined from a best fit to the low-lying positive-parity level energies of even-even $^{148-154}$Sm in the IBM-CM and the CQ formalism, where the unit is in MeV, except for the dimensionless parameter χ and the effective charge q_2 (in $\sqrt{\mathrm{W.u.}}$), and $\chi = -\sqrt{7/2}$ is preferred for all the nuclei fitted in the CQ formalism.

		$^{148}_{62}\mathrm{Sm}_{86}$	$^{150}_{62}\mathrm{Sm}_{88}$	$^{152}_{62}\mathrm{Sm}_{90}$	$^{154}_{62}\mathrm{Sm}_{92}$
IBM-CM	$\epsilon_d^{(N)} - \epsilon_s^{(N)}$	0.93000	0.88000	0.71440	0.66000
	$\kappa^{(N)}$	0.03014	0.03022	0.03222	0.03224
	$\epsilon_s^{(N+2)}$	−0.54058	−0.43760	−0.40162	−0.36849
	$\epsilon_d^{(N+2)} - \epsilon_s^{(N+2)}$	0.11300	0.11000	0.10800	0.10400
	$\kappa^{(N+2)}$	0.01000	0.01300	0.01350	0.01390
	b	0.00770	0.00760	0.00290	0.00055
	χ	−0.88000	−0.92000	−0.93000	−0.94000
	ω	0.03120	0.03150	0.03355	0.05011
	q_2	1.49330	1.69880	2.10015	2.03651
CQ	$\epsilon_d - \epsilon_s$	0.61000	0.48000	0.44000	0.32880
	κ	0.01000	0.01007	0.01400	0.01866
	q_2	1.72300	1.99340	2.15900	1.85000

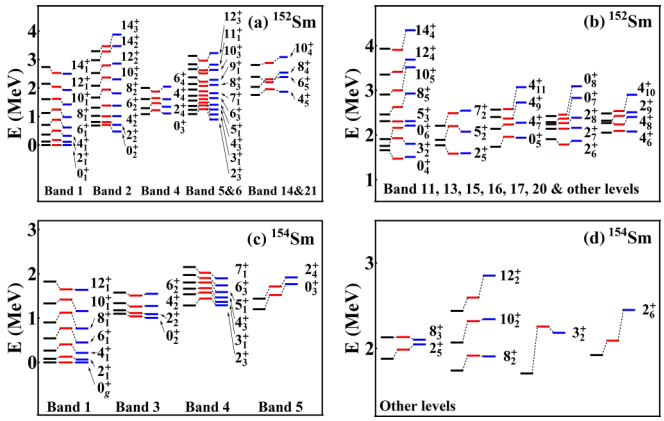

FIG. 2. The same as Fig. 1, but for ^{152}Sm and ^{154}Sm.

in the fitting. For ^{154}Sm, there are 26 positive-parity levels fitted as shown in Figs. 2(c) and 2(d), among which spin and parity of the excited levels at 2.130 MeV have not been determined experimentally and are assigned to be 8_3^+ in the fitting. In addition, spin and parity of several excited levels have not been confirmed uniquely, for which the spin and parity assignments in both the IBM-CM and the CQ formalism are clearly provided in Tables III–VI. As clearly shown by $\sigma(E)$ provided in Table VII, the fitting quality of the IBM-CM to the positive-parity level energies of these nuclei is significantly better than that of the CQ formalism.

Once the model parameters are determined in the fitting to the level energies, experimentally known $B(E2)$ values of ^{148,150,152,154}Sm are calculated accordingly, of which the results are shown in Table VIII. In both the IBM-CM and the CQ formalism, the effective charge related parameter q_2 is fixed by the experimental value of $B(E2;2_1^+ \to 0_1^+)$, which is provided for each nucleus in the last row of Table II. For ^{148}Sm, the calculated results of the IBM-CM are closer to the corresponding experimental values than those of the CQ formalism except for $B(E2;2_2^+ \to 2_1^+)$. For ^{154}Sm, the calculated results of $B(E2;8_1^+ \to 6_1^+)$ and $B(E2;10_1^+ \to 8_1^+)$ of the IBM-CM are significantly improved in comparison to the corresponding results of the CQ formalism. For ^{150}Sm, the calculated results of the IBM-CM are better than those of the CQ formalism except for $B(E2;4_1^+ \to 2_1^+)$, $B(E2;6_1^+ \to 4_1^+)$, $B(E2;4_2^+ \to 2_3^+)$, $B(E2;4_3^+ \to 2_1^+)$, and $B(E2;4_4^+ \to 2_2^+)$. Especially, $B(E2;0_2^+ \to 2_1^+)$, $B(E2;2_2^+ \to 0_2^+)$, $B(E2;4_2^+ \to 2_2^+)$, and $B(E2;4_2^+ \to 6_1^+)$ are significantly improved in comparison to those calculated from the CQ formalism, which is mainly due to the fact that the 0_2^+, 2_2^+, 4_2^+, and 6_1^+ states of ^{150}Sm are intruder configuration dominant as shown by the occupation probabilities of the normal and intruder configurations of these states in Fig. 4(b). For example, since the 0_2^+ state mainly belongs to the intruder configuration, while the 2_1^+ state mainly belongs to the normal configuration in the IBM-CM, $B(E2;0_2^+ \to 2_1^+)$ turns to be greatly suppressed and becomes closer to the corresponding experimental value in comparison to the value of the CQ formalism without the configuration mixing. Similarly, for ^{152}Sm, $B(E2;2_2^+ \to 0_2^+)$, $B(E2;4_2^+ \to 2_2^+)$, $B(E2;8_1^+ \to 6_1^+)$, $B(E2;0_2^+ \to 2_1^+)$, and $B(E2;0_3^+ \to 2_2^+)$ in the IBM-CM are also significantly improved in comparison to the CQ formalism, which is mainly due to the fact that the 0_2^+, 2_2^+, 4_2^+, 6_1^+, and 8_1^+ states are intruder configuration dominant as shown by the occupation probabilities of the normal and intruder configurations of these states in Fig. 4(c). As shown by $\sigma[B(E2)]$ in Table VII, the calculated results of the IBM-CM are obviously better than those of the CQ formalism due to the configuration mixing in these nuclei.

TABLE III. Some low-lying positive-parity level energies of ^{148}Sm (in MeV), where " Theory " denotes both the IBM-CM and the CQ formalism, " — " indicates that the corresponding spin and parity are not determined in experiments, and the experimental data are taken from Ref. [45].

Spin and parity				
Theory	Expt.	Expt.	IBM-CM	CQ
0_1^+	0^+	0	0	0
0_2^+	0^+	1.424	1.243	0.929
0_3^+	0^+	1.921	1.636	1.688
0_4^+	0^+	2.205	1.969	2.078
0_5^+	0^+	2.358	2.217	2.857
0_6^+	—	2.441	2.361	3.368
2_1^+	2^+	0.550	0.540	0.466
2_2^+	2^+	1.454	1.439	1.045
2_3^+	2^+	1.664	1.648	1.499
2_4^+	2^+	1.972	2.018	2.139
2_5^+	2^+	2.146	2.064	2.308
2_6^+	$(1,2^+)$	2.284	2.281	2.718
2_7^+	2^+	2.314	2.361	2.990
2_8^+	2^+	2.382	2.430	3.413
2_9^+	(2^+)	2.442	2.547	3.546
2_{10}^+	2^+	2.568	2.671	4.074
3_1^+	3^+	1.904	2.013	1.625
3_2^+	3^+	2.328	2.421	2.785
3_3^+	3^+	2.390	2.604	3.685
4_1^+	4^+	1.180	1.212	0.964
4_2^+	4^+	1.733	1.832	1.607
4_3^+	4^+	1.895	2.146	2.096
4_4^+	4^+	2.111	2.282	2.259
4_5^+	4^+	2.228	2.373	2.795
4_6^+	4^+	2.327	2.544	2.949
4_7^+	4^+	2.490	2.642	3.387
4_8^+	4^+	2.524	2.696	3.492
4_9^+	4^+	2.673	2.732	3.671
4_{10}^+	4^+	2.724	2.819	4.139
5_1^+	5^+	2.148	2.342	2.217
5_2^+	5^+	2.214	2.680	2.917
5_3^+	5^+	2.641	2.823	3.461
6_1^+	6^+	1.906	1.917	1.500
6_2^+	6^+	2.096	2.260	2.202
6_3^+	6^+	2.194	2.517	2.724
6_4^+	$(4^+,5,6^+)$	2.716	2.610	2.901
7_1^+	7^+	2.392	2.722	2.842
8_1^+	8^+	2.545	2.430	2.080
8_2^+	8^+	2.715	2.881	2.834
9_1^+	$9^{(+)}$	3.095	3.192	3.506

TABLE IV. The same as Table III, but for ^{150}Sm.

Spin and parity				
Theory	Expt.	Expt.	IBM-CM	CQ
0_1^+	0^+	0	0	0
0_2^+	0^+	0.740	0.761	0.595
0_3^+	0^+	1.256	1.229	1.261
2_1^+	2^+	0.334	0.372	0.291
2_2^+	2^+	1.046	0.921	0.756
2_3^+	2^+	1.194	1.312	1.034
2_4^+	2^+	1.417	1.568	1.540
2_5^+	2^+	1.794	1.596	1.745
2_6^+	(2^+)	1.927	1.938	1.987
2_7^+	2^+	2.006	2.055	2.297
2_8^+	$(2^+, 5^+)$	2.055	2.115	2.540
2_9^+	$2^+, 3^+, 4^+$	2.342	2.263	2.688
2_{10}^+	$(1^-, 2^+)$	2.507	2.393	3.053
3_1^+	3^+	1.505	1.534	1.188
3_2^+	$(3^+, 4^+)$	2.044	2.049	2.044
3_3^+	3^+	2.456	2.361	2.850
3_4^+	$3^+, 4^+$	2.556	2.647	3.098
4_1^+	4^+	0.773	0.852	0.620
4_2^+	4^+	1.449	1.224	1.164
4_3^+	4^+	1.643	1.669	1.486
4_4^+	4^+	1.820	1.808	1.691
4_5^+	4^+	1.971	2.061	2.063
4_6^+	4^+	2.025	2.186	2.240
4_7^+	4^+	2.117	2.319	2.505
4_8^+	4^+	2.153	2.364	2.621
4_9^+	4^+	2.191	2.423	2.835
4_{10}^+	$3^+, 4^+$	2.465	2.570	3.125
5_1^+	$2^+, 5^+$	1.883	1.830	1.624
5_2^+	5^+	2.020	2.325	2.205
5_3^+	—	2.444	2.452	2.578
6_1^+	6^+	1.279	1.302	0.999
6_2^+	$(6)^+$	2.107	1.792	1.606
8_1^+	8^+	1.837	1.757	1.428
10_1^+	10^+	2.433	2.292	1.905
12_1^+	12^+	3.048	2.922	2.429
14_1^+	14^+	3.676	3.651	3.000
16_1^+	16^+	4.306	4.482	3.615

Figure 3 provides four typical $B(E2)$ values and the branching ratio $R = B(E2; 2_3^+ \to 0_2^+)/B(E2; 2_3^+ \to 0_1^+)$ [42,43] as functions of the mass number A for ^{148,150,152,154}Sm. For $B(E2; 0_2^+ \to 2_1^+)$ shown in Fig. 3(a), the IBM-CM result is significantly improved in comparison to that of the CQ formalism, except for ^{154}Sm, of which the IBM-CM result is larger than the experimental one. For $B(E2; 2_2^+ \to 0_1^+)$ shown in Fig. 3(b), the results of both the models are strongly suppressed and about the same in magnitude, and the IBM-CM result seems better than that of the CQ formalism, though the experimental value of $B(E2; 2_2^+ \to 0_1^+)$ for ^{154}Sm is not available. In Ref. [42], the ratio R was found to be very small for ^{152}Sm and could be reproduced in the CQ formalism, which was then interpreted due to the phase coexistence [43]. In the present work, however, the parameters of both the models were

TABLE V. The same as Table III, but for ^{152}Sm.

Spin and parity				
Theory	Expt.	Expt.	IBM-CM	CQ
0_1^+	0^+	0	0	0
0_2^+	0^+	0.685	0.706	0.474
0_3^+	0^+	1.083	1.223	1.108
0_4^+	0^+	1.659	1.470	1.509
0_5^+	0^+	1.736	1.960	1.939
0_6^+	0^+	1.755	2.160	2.273
0_7^+	$0, 1, 2, 3^-$	2.287	2.366	2.830
0_8^+	–	2.423	2.455	3.090
2_1^+	2^+	0.122	0.176	0.114
2_2^+	2^+	0.810	0.807	0.708
2_3^+	2^+	1.086	1.257	0.895
2_4^+	2^+	1.293	1.471	1.342
2_5^+	2^+	1.769	1.583	1.591
2_6^+	2^+	1.906	1.786	1.868
2_7^+	2^+	2.138	2.141	2.160
2_8^+	2^+	2.240	2.266	2.386
2_9^+	2^+	2.268	2.427	2.509
3_1^+	3^+	1.234	1.389	1.073
3_2^+	(3^+)	1.908	1.928	1.803
4_1^+	4^+	0.366	0.505	0.323
4_2^+	4^+	1.023	1.009	1.014
4_3^+	4^+	1.372	1.490	1.247
4_4^+	4^+	1.613	1.646	1.607
4_5^+	4^+	1.757	1.958	1.870
4_6^+	4^+	2.052	2.091	2.077
4_7^+	$(2^+, 3, 4^+)$	2.138	2.235	2.274
4_8^+	$4^+, 5$	2.320	2.236	2.403
4_9^+	$3, 4^+$	2.402	2.367	2.727
4_{10}^+	3,4,5	2.482	2.536	2.901
4_{11}^+	$4^+, 5$	2.567	2.579	3.070
5_1^+	5^+	1.560	1.612	1.414
5_2^+	5^+	1.891	2.199	2.074
5_3^+	—	2.309	2.304	2.310
6_1^+	6^+	0.707	0.887	0.616
6_2^+	6^+	1.311	1.385	1.382
6_3^+	6^+	1.728	1.740	1.646
6_4^+	6^+	2.004	1.876	2.049
6_5^+	6^+	2.040	2.307	2.385
7_1^+	7^+	1.946	1.886	1.818
7_2^+	7^+	2.206	2.487	2.545
8_1^+	8^+	1.125	1.246	0.985
8_2^+	8^+	1.666	1.945	1.813
8_3^+	8^+	2.140	2.074	2.110
8_4^+	8^+	2.392	2.204	2.541
8_5^+	8^+	2.459	2.625	2.928
9_1^+	9^+	2.375	2.221	2.288
10_1^+	10^+	1.609	1.621	1.424
10_2^+	10^+	2.080	2.369	2.305
10_3^+	10^+	2.662	2.513	2.637
10_4^+	(10^+)	2.810	2.879	3.086
10_5^+	10^+	2.905	2.999	3.516
11_1^+	11^+	2.833	2.622	2.820
12_1^+	12^+	2.149	2.045	1.931
12_2^+	12^+	2.526	2.795	2.858
12_3^+	12^+	3.128	2.960	3.226
12_4^+	12^+	3.352	3.414	3.687

TABLE V. *(Continued.)*

Spin and parity				
Theory	Expt.	Expt.	IBM-CM	CQ
14_1^+	14^+	2.736	2.529	2.502
14_2^+	14^+	2.977	3.280	3.471
14_3^+	14^+	3.293	3.469	3.876
14_4^+	14^+	3.931	3.905	4.344

determined by the least-mean-square algorithm, in which no special attention was paid to this ratio. As shown in Fig. 3(c), $B(E2;2_3^+ \to 0_2^+)$ and $B(E2;2_3^+ \to 0_1^+)$ produced from the two models are all acceptable, but the IBM-CM results are a little improved. As clearly shown in Fig. 3(d), the ratio R indeed decreases drastically from ^{150}Sm to ^{152}Sm in both the models, but the IBM-CM result is closer to the experimental data globally, though the experimental ratios of ^{148}Sm and ^{154}Sm are not available. The calculated results for the experimentally known electric quadrupole moments of the 2_1^+ and 4_1^+ states in ^{148,150,152,154}Sm are provided in Table IX, which shows once again that the IBM-CM results are closer to the experimental data in comparison to the corresponding results of the IBM-CQ formalism.

TABLE VI. The same as Table III, but for ^{154}Sm.

Spin and parity				
Theory	Expt.	Expt.	IBM-CM	CQ
0_1^+	0^+	0	0	0
0_2^+	0^+	1.099	1.040	1.006
0_3^+	0^+	1.202	1.522	1.768
2_1^+	2^+	0.082	0.130	0.065
2_2^+	2^+	1.178	1.115	1.091
2_3^+	2^+	1.286	1.443	1.290
2_4^+	2^+	1.440	1.715	1.920
2_5^+	2^+	1.878	1.986	2.047
2_6^+	2^+	1.922	2.091	2.450
3_1^+	3^+	1.539	1.578	1.367
3_2^+	3^+	1.707	2.219	2.183
4_1^+	4^+	0.267	0.408	0.216
4_2^+	4^+	1.338	1.263	1.276
4_3^+	4^+	1.665	1.677	1.468
5_1^+	5^+	1.805	1.805	1.589
6_1^+	6^+	0.544	0.772	0.451
6_2^+	6^+	1.577	1.510	1.550
6_3^+	(6^+)	1.974	1.905	1.740
7_1^+	7^+	2.154	2.023	1.899
8_1^+	8^+	0.903	1.124	0.767
8_2^+	(8^+)	1.741	1.916	1.907
8_3^+	—	2.130	2.133	2.102
10_1^+	10^+	1.333	1.420	1.160
10_2^+	(10^+)	2.069	2.319	2.342
12_1^+	12^+	1.826	1.698	1.639
12_2^+	(12^+)	2.439	2.595	2.852

TABLE VII. The root-mean-square deviations of the positive-parity level energies (in MeV) and B(E2) values (in W.u.).

	$^{148}_{62}$Sm$_{86}$	$^{150}_{62}$Sm$_{88}$	$^{152}_{62}$Sm$_{90}$	$^{154}_{62}$Sm$_{92}$
$\sigma_{\rm CM}(E)$	0.19	0.15	0.17	0.23
$\sigma_{\rm CQ}(E)$	0.66	0.39	0.26	0.29
$\sigma_{\rm CM}[B(E2)]$	3.75	23.00	27.01	27.79
$\sigma_{\rm CQ}[B(E2)]$	4.04	48.18	32.84	31.57

The histograms shown in Fig. 4 are occupation probabilities of the normal and intruder configurations in some excited states of ^{148,150,152,154}Sm described by the IBM-CM according to Eqs. (10) and (11). It is clearly shown that the 0_2^+, 2_2^+, and 4_2^+ states are always the intruder configuration dominant states, except for ^{148}Sm, of which, instead of 0_2^+ and 2_2^+ states, the 0_3^+ and 2_3^+ states become the intruder configuration dominant states. Due to the intruder configuration dominance in these states, the related $B(E2)$ values, such as $B(E2;0_2^+ \to 2_1^+)$, $B(E2;2_2^+ \to 0_2^+)$, and $B(E2;4_2^+ \to 2_2^+)$ of these nuclei, are fitted better in the IBM-CM formalism than in the CQ formalism. In addition, the occupation probabilities of the normal and intruder configurations of 0_2^+ and 0_3^+ states are always opposite. For example, the occupation probabilities of the normal and the intruder configurations of the 0_2^+ states are 18% and 82%, respectively, while they are 82% and 18%, respectively, in the 0_3^+ states of ^{152}Sm. Moreover, if the β-band-head 0^+ state is assumed to be the normal configuration dominated in the IBM-CM, according to Fig. 4, the 0_2^+ state in ^{148}Sm, and the 0_3^+ state in ^{150,152,154}Sm may be the β-band-head with 74%, 80%, 82%, and 66% normal configuration contribution, respectively. Most noticeably, the occupation probabilities of the normal and intruder configurations of the yrast states change gradually from normal configuration dominant to intruder configuration dominant with the increasing of the angular momentum quantum number L, among which the 6_1^+ state is the crossover point. Figure 5 provides $B(E2;L \to$

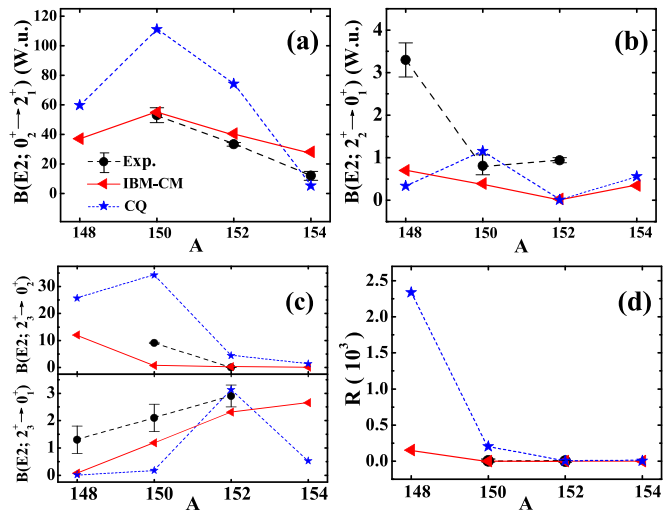

FIG. 3. Four typical $B(E2)$ values and the ratio $R = B(E2;2_3^+ \to 0_2^+)/B(E2;2_3^+ \to 0_1^+)$ of ^{148,150,152,154}Sm.

TABLE VIII. $B(E2)$ values calculated from the IBM-CM and the CQ formalism and compared with the experimentally available data (in W.u.), where "—" indicates that the corresponding experimental value is not available.

	$L_\xi \to L'_{\xi'}$	Expt. [45]	IBM-CM	CQ	$L_\xi \to L'_{\xi'}$	Expt. [45]	IBM-CM	CQ
^{148}Sm	$2_1^+ \to 0_1^+$	31.2(13)	31.200	31.200	$2_2^+ \to 0_1^+$	3.3(4)	0.598	0.338
	$4_1^+ \to 2_1^+$	51(6)	52.662	57.445	$2_2^+ \to 2_1^+$	30(3)	21.903	35.294
	$2_3^+ \to 0_1^+$	1.3(5)	0.078	0.011	$2_3^+ \to 2_1^+$	4.5(15)	1.788	0.112
	$2_3^+ \to 0_2^+$	—	11.991	25.691	$0_2^+ \to 2_1^+$	—	37.108	59.681
^{150}Sm	$2_1^+ \to 0_1^+$	57.1(13)	57.100	57.100	$4_1^+ \to 2_1^+$	110(17)	93.278	107.922
	$6_1^+ \to 4_1^+$	150(5)	125.209	137.564	$8_1^+ \to 6_1^+$	170(9)	175.827	150.798
	$0_2^+ \to 2_1^+$	53(5)	54.894	110.980	$2_2^+ \to 0_1^+$	$0.81^{+0.26}_{-0.21}$	0.389	1.154
	$2_2^+ \to 0_2^+$	110^{+4}_{-3}	99.999	31.334	$4_2^+ \to 2_2^+$	190(9)	126.935	62.159
	$4_2^+ \to 2_3^+$	42(20)	2.786	13.911	$4_2^+ \to 6_1^+$	80(4)	76.750	14.154
	$2_3^+ \to 0_2^+$	9.1(24)	0.740	34.227	$2_3^+ \to 4_1^+$	7(3)	0.376	27.652
	$2_3^+ \to 0_1^+$	2.1(5)	1.187	0.170	$4_3^+ \to 2_1^+$	1.4(7)	0.030	0.104
	$4_3^+ \to 2_4^+$	70(4)	24.694	2.733	$4_4^+ \to 2_2^+$	4.1(21)	0.011	0.928
^{152}Sm	$2_1^+ \to 0_1^+$	145.0(16)	145.000	145.000	$4_1^+ \to 2_1^+$	209.5(22)	215.436	222.469
	$6_1^+ \to 4_1^+$	240(4)	245.296	251.032	$8_1^+ \to 6_1^+$	293(4)	299.958	259.356
	$10_1^+ \to 8_1^+$	314^{+35}_{-26}	328.409	253.543	$0_2^+ \to 2_1^+$	33.3(12)	40.434	74.149
	$2_2^+ \to 0_2^+$	170(12)	198.643	90.852	$2_2^+ \to 2_1^+$	5.7(4)	4.199	13.459
	$2_2^+ \to 4_1^+$	18.0(12)	48.513	23.395	$2_2^+ \to 0_1^+$	0.94(6)	0.032	0.006
	$4_2^+ \to 2_2^+$	250(4)	270.711	142.633	$4_2^+ \to 6_1^+$	17(3)	92.452	15.447
	$4_2^+ \to 2_1^+$	0.74(12)	2.095	0.070	$4_2^+ \to 4_1^+$	$5.0^{+1}_{-0.7}$	4.947	10.117
	$3_1^+ \to 2_3^+$	120^{+6}_{-9}	230.693	157.147	$3_1^+ \to 2_1^+$	$6.8^{+1.5}_{-1.1}$	3.173	3.726
	$3_1^+ \to 4_1^+$	$7.2^{+1.6}_{-1.1}$	4.345	4.386	$2_3^+ \to 0_1^+$	2.9(4)	2.310	3.127
	$2_3^+ \to 0_2^+$	0.026(4)	0.284	4.401	$2_3^+ \to 4_1^+$	0.56(8)	0.394	6.496
	$4_3^+ \to 2_3^+$	62^{+35}_{-24}	87.341	68.956	$4_3^+ \to 2_2^+$	$0.30^{+0.18}_{-0.13}$	0.591	1.546
	$4_3^+ \to 6_1^+$	$0.9^{+0.6}_{-0.4}$	1.593	6.544	$4_3^+ \to 2_1^+$	$0.7^{+0.5}_{-0.3}$	0.234	0.843
	$4_3^+ \to 4_1^+$	7^{+4}_{-3}	5.770	1.856	$0_3^+ \to 2_2^+$	34^{+23}_{-11}	57.47	110.27
	$0_3^+ \to 2_1^+$	$0.80^{+0.53}_{-0.23}$	9.850	0.881	$2_5^+ \to 4_3^+$	40^{+13}_{-12}	33.995	23.599
	$2_5^+ \to 0_2^+$	$7.6^{+2.2}_{-2.0}$	0.808	0.644	$2_5^+ \to 0_1^+$	$0.58^{+0.16}_{-0.15}$	0.106	0.013
^{154}Sm	$2_1^+ \to 0_1^+$	176(1)	176.000	176.000	$4_1^+ \to 2_1^+$	245(6)	255.640	247.716
	$6_1^+ \to 4_1^+$	289(8)	285.971	265.010	$8_1^+ \to 6_1^+$	319(17)	315.000	265.142
	$10_1^+ \to 8_1^+$	314(16)	340.219	255.270	$12_1^+ \to 10_1^+$	282(19)	358.560	237.685
	$0_2^+ \to 2_1^+$	12(3)	28.139	5.188	$2_4^+ \to 0_1^+$	2.13(16)	0.418	0.001
	$2_4^+ \to 4_1^+$	0.48(7)	0.178	0.015	$2_2^+ \to 0_1^+$	-	0.347	0.561
	$2_3^+ \to 0_1^+$	-	2.652	0.526	$2_3^+ \to 0_2^+$	-	0.128	1.353

$L-2$) along the yrast line as a function of L of ^{152,154}Sm in the IBM-CM in comparison to that in the CQ formalism. It is shown that the IBM-CM curves are closer to the experimental data in general, except for the tail at $L=12$ of ^{154}Sm, which is still away from the experimental point, while the CQ curves are always much lower than the experimental data points of ^{152}Sm and ^{154}Sm for $L \geqslant 6$. Therefore, the IBM-CM significantly improves the results of most $B(E2)$ values not

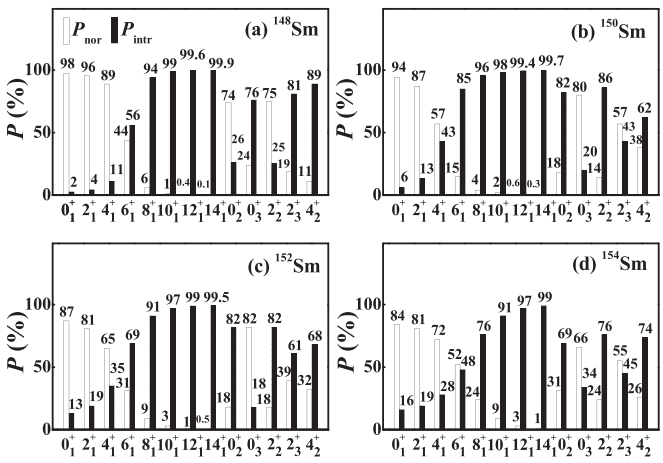

FIG. 4. The same as Fig. 1, but for ^{152}Sm and ^{154}Sm.

TABLE IX. The electric quadrupole moments $Q(2_1^+)$ and $Q(4_1^+)$ (in e b), where "—" indicates that the corresponding experimental value is not available.

		$^{148}_{62}$Sm$_{86}$	$^{150}_{62}$Sm$_{88}$	$^{152}_{62}$Sm$_{90}$	$^{154}_{62}$Sm$_{92}$
$Q(2_1^+)$	Expt. [45]	−0.98(27)	−1.32(19)	−1.683(18)	−1.87(4)
	IBM-CM	−0.837	−1.335	−2.190	−2.336
	CQ	−0.784	−1.293	−2.235	−2.440
$Q(4_1^+)$	Expt. [45]	—	—	−2.6(14)	−2.2(8)
	IBM-CM	−1.255	−2.103	−3.023	−2.908
	CQ	−1.357	−2.039	−3.100	−3.200

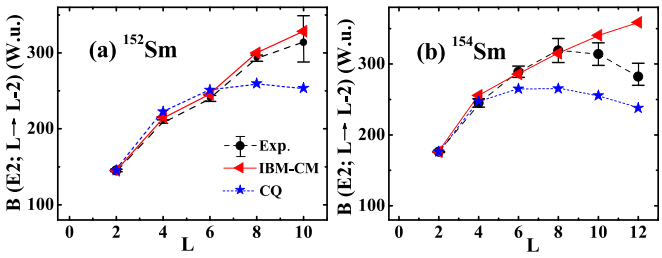

FIG. 5. $B(E2; L \to L-2)$ along the yrast line as a function of L of ^{152,154}Sm in the IBM-CM with comparison to the experimental data and the CQ formalism data.

only due to the inclusion of the intruder configuration but also due to the symmetry structure of the normal and intruder configurations in the IBM-CM eigenstates shown in Fig. 4. All in all, the 2p-2h cross-shell excitations seem of importance in elucidating the low-lying structures of these well-deformed nuclei.

IV. CONCLUSIONS

In summary, the IBM-CM including 2p-2h excitations across the closed shell is applied to describe well-deformed ^{148,150,152,154}Sm focusing on the cross-shell excitation effects in these nuclei. Experimentally known positive-parity level energies, $B(E2)$ values, and electric quadrupole moments are fitted and compared with the corresponding experimental data and the results of the consistent-Q formalism. It is shown that the IBM-CM is better than the CQ formalism in general. Especially, the $B(E2)$ values, such as $B(E2; 0_2^+ \to 2_1^+)$, $B(E2; 2_2^+ \to 0_2^+)$, and $B(E2; 4_2^+ \to 2_2^+)$, of these nuclei produced from the IBM-CM are significantly improved in comparison to those from the CQ formalism. The occupation probabilities of the intruder and the normal configuration calculated from the IBM-CM show that the 0_2^+, 2_2^+, and 4_2^+ states of ^{150,152,154}Sm are intruder configuration dominant, which reveals the nature of these low-lying states in ^{150,152,154}Sm in the IBM-CM framework, namely, the 2p-2h excitations indeed play an important role in these nuclei. Moreover, the IBM-CM results also show that the occupation probabilities of the normal and intruder configurations of the yrast states change gradually from normal configuration dominant to intruder configuration dominant with the increasing of the angular momentum quantum number, among which the 6_1^+ state is the crossover point. $B(E2; L \to L-2)$ along the yrast line of ^{152,154}Sm produced from the IBM-CM is indeed closer to the experimental data than that from the CQ formalism without configuration mixing. Furthermore, in order to describe the isoscalar giant monopole and quadrupole resonance phenomena in these well-deformed nuclei, 1p-1h excitations also approximated as bosons may be included as proposed in Ref. [28], which will be a part of our future work.

ACKNOWLEDGMENTS

Support from the National Natural Science Foundation of China (Grant No. 12175097) and from LSU through its Sponsored Research Rebate Program as well as under the LSU Foundation's Distinguished Research Professorship Program is acknowledged.

[1] F. Iachello and A. Arima, *The Interacting Boson Model* (Cambridge University, Cambridge, England, 1987).
[2] F. Dickmann and K. Dietrich, Z. Phys. **271**, 417 (1974).
[3] P. Paradis, G. Lamoureux, R. Lecomte, and S. Monaro, Phys. Rev. C **14**, 835 (1976).
[4] P. D. Duval and B. R. Barrett, Phys. Lett. B **100**, 223 (1981).
[5] P. D. Duval and B. R. Barrett, Nucl. Phys. A **376**, 213 (1982).
[6] K. Heyde, P. Van Isacker, M. Waroquier, G. Wenes, and M. Sambataro, Phys. Rev. C **25**, 3160 (1982).
[7] K. Heyde, P. Van Isacker, M. Waroquier, J. Wood, and R. Meyer, Phys. Rep. **102**, 291 (1983).
[8] K. Heyde and J. L. Wood, Rev. Mod. Phys. **83**, 1467 (2011).
[9] K. Heyde, J. Jolie, P. Van Isacker, J. Moreau, and M. Waroquier, Phys. Rev. C **29**, 1428 (1984).
[10] A. Frank, P. Van Isacker, and C. E. Vargas, Phys. Rev. C **69**, 034323 (2004).
[11] A. Frank, P. Van Isacker, and F. Iachello, Phys. Rev. C **73**, 061302(R) (2006).
[12] N. Gavrielov, A. Leviatan, and F. Iachello, Phys. Rev. C **105**, 014305 (2022).
[13] N. Gavrielov, A. Leviatan, and F. Iachello, Phys. Rev. C **106**, L051304 (2022).
[14] E. Maya-Barbecho, S. Baid, J. M. Arias, and J. E. García-Ramos, Phys. Rev. C **108**, 034316 (2023).
[15] N. Gavrielov, Phys. Rev. C **108**, 014320 (2023).
[16] J. E. García-Ramos and K. Heyde, Nucl. Phys. A **825**, 39 (2009).
[17] J. E. García-Ramos and K. Heyde, Phys. Rev. C **89**, 014306 (2014).
[18] J. E. García-Ramos and K. Heyde, Phys. Rev. C **102**, 054333 (2020).
[19] J. E. García-Ramos, J. Arias, and A. Vitturi, Chin. Phys. C **44**, 124101 (2020).
[20] J. E. García-Ramos, K. Heyde, L. M. Robledo, and R. Rodríguez-Guzmán, Phys. Rev. C **89**, 034313 (2014).
[21] A. K. Singh, G. Gangopadhyay, and D. Banerjee, Phys. Rev. C **55**, 968 (1997).
[22] M. Sambataro and G. Molnar, Nucl. Phys. A **376**, 201 (1982).
[23] C. De Coster, K. Heyde, B. Decroix, P. Van Isacker, J. Jolie, H. Lehmann, and J. Wood, Nucl. Phys. A **600**, 251 (1996).
[24] F. Pan, D. Li, G. Cheng, Z. Qiao, J. Bai, and J. P. Draayer, Phys. Rev. C **97**, 034316 (2018).
[25] F. Pan, S. Yuan, Z. Qiao, J. Bai, Y. Zhang, and J. P. Draayer, Phys. Rev. C **97**, 034326 (2018).
[26] L. Dai, F. Pan, Z. Feng, Y. Zhang, S. Cui, and J. P. Draayer, Chin. Phys. C **44**, 064102 (2020).
[27] K. Nomura, T. Otsuka, and P. Van Isacker, J. Phys. G: Nucl. Part. Phys. **43**, 024008 (2016).

[28] F. Pan, Y. Zhang, L. Dai, J. P. Draayer, and D. Kekejian, Phys. Lett. B **848**, 138340 (2024).
[29] Y. Wu, A. Li, F. Pan, L. Dai, and J. P. Draayer, Symmetry **14**, 2620 (2022).
[30] P. E. Garrett, J. Phys. G: Nucl. Part. Phys. **27**, R1 (2001).
[31] P. E. Garrett, W. D. Kulp, J. L. Wood, D. Bandyopadhyay, S. Choudry, D. Dashdorj, S. R. Lesher, M. T. McEllistrem, M. Mynk, J. N. Orce *et al.*, Phys. Rev. Lett. **103**, 062501 (2009).
[32] O. Scholten, F. Iachello, and A. Arima, Ann. Phys. **115**, 325 (1978).
[33] P. D. Duval, D. Goutte, and M. Vergnes, Phys. Lett. B **124**, 297 (1983).
[34] M. Harder, K. Tang, and P. Van Isacker, Phys. Lett. B **405**, 25 (1997).
[35] D. D. Warner and R. F. Casten, Phys. Rev. C **28**, 1798 (1983).
[36] G. Rosensteel, Phys. Rev. C **41**, 730 (1990).
[37] Y. Akiyama and J. Draayer, Comput. Phys. Commun. **5**, 405 (1973).
[38] J. Draayer and Y. Akiyama, J. Math. Phys. **14**, 1904 (1973).
[39] W.-T. Chou, N. V. Zamfir, and R. F. Casten, Phys. Rev. C **56**, 829 (1997).
[40] Y. Zhang and F. Iachello, Phys. Rev. C **95**, 034306 (2017).
[41] K. Nomura and Y. Zhang, Phys. Rev. C **99**, 024324 (2019).
[42] R. F. Casten, M. Wilhelm, E. Radermacher, N. V. Zamfir, and P. von Brentano, Phys. Rev. C **57**, R1553 (1998).
[43] F. Iachello, N. V. Zamfir, and R. F. Casten, Phys. Rev. Lett. **81**, 1191 (1998).
[44] P. Moller, A. Sierk, T. Ichikawa, and H. Sagawa, At. Data Nucl. Data Tables **109-110**, 1 (2016).
[45] National Nuclear Data Center, Brookhaven National Laboratory, NuDat3.0 (nuclear structure and decay data), https://www.nndc.bnl.gov/nudat3/.